Electronic Supplementary Information

Discrete evolution of the crystal structure during the growth of Ba-hexaferrite nanoplatelets

D. Makovec,* B. Belec, T. Goršak, D. Lisjak, M. Komelj, G. Dražić and S. Gyergyek

Materials

Iron (III) nitratehepta hydrate ($Fe(NO_3)_3 \cdot H_2O$, barium nitrate ($Ba(NO_3)_2$), sodium hydroxide (NaOH), nitric acid (HNO_3), ammonia solution (NH_3, 25%), tetraethyl orthosilicate (TEOS) were purchased from Alfa Aesar.

Characterization

For the transmission (TEM) and scanning-transmission (STEM) electron microscopy studies, the nanoplatelets were deposited on a copper-grid-supported lacy carbon foil. When the stable aqueous suspension was dried on the TEM grid, the nanoplatelets deposited almost exclusively flat on the support. For the structural analysis, the nanoplatelets were suspended in ethanol, where they slowly aggregated. In the small aggregates deposited on the specimen support a much larger number of nanoplatelets was found oriented edge-on, with their basal surfaces parallel to the electron beam. TEM analyses were performed using a field-emission electron-source TEM Jeol 2010F equipped with an Oxford Instruments ISIS300 energy-dispersive x-ray spectroscopy (EDXS) detector operated at 200 kV. For the STEM analyses a probe Cs-corrected Jeol ARM 200CF STEM was operated at 80 kV. During the analysis of the samples, HAADF and ABF detectors were used simultaneously at 68–180 and 10–16 mrad collection semi angles, respectively. To minimize the specimen drift, images were taken several hours after the insertion of the sample in the microscope and at least 20 minutes after the last sample positioning to minimize the goniometer drift. The chemical composition was analysed using a Jeol Centurio EDXS system with 100 mm^2 SDD detector and Gatan GIF Quantum ER Dual EELS system. The EELS spectra for the determination of the valence state of the iron cations in the nanoplatelets were collected in STEM mode using a 24-mrad convergence and 60-mrad collection semi-angles. Low-loss and core-loss spectra were acquired simultaneously using the Dual-EELS

option of the system. Before quantification the spectra were corrected for plural scattering in order to reduce the influence of the thickness. The Fe valence state was determined based on the energy difference ΔE between the onset energy of the O-K and Fe-L3 edges.[S1] The onset energy was defined at 10 % of the edge maxima. The calibration curve (ΔE vs. Fe valence state) was derived from the EELS spectra of the standards, as shown in Table SI1). Each experimental ΔE was the average of 5–10 measurements.

The magnetic properties at room temperature were measured using a vibrating-sample magnetometer (VSM). To avoid the problem of the unknown orientation of the nanoplatelets and to minimize the dipole-dipole interactions, the specimens for the VSM measurements were prepared by mixing the nanoplatelets (~1 mg) with sucrose (0.5 g). The mixture was uniaxially pressed into cubic compacts. The magnetizations of the cubic compacts containing the nanoplatelets were measured with the magnetic field applied in the three normal directions of the cube. The three measurements were averaged to obtain the magnetic properties of the "randomly oriented" nanoplatelets.
The temperature dependence of the magnetization for sample powders was determined under zero-field cooling (ZFC) and field cooling (FC) (H=100 Oe) conditions in the temperature range between 2 K and 300 K using a SQUID.

Annealing of the nanoplatelets

After the synthesis the BF80 nanoplatelets were thoroughly washed with dilute nitric acid and with water. The washed nanoplatelets were dried in a vacuum at room temperature. The powder was annealed for 2 hours at 700 ^{o}C in ambient air.

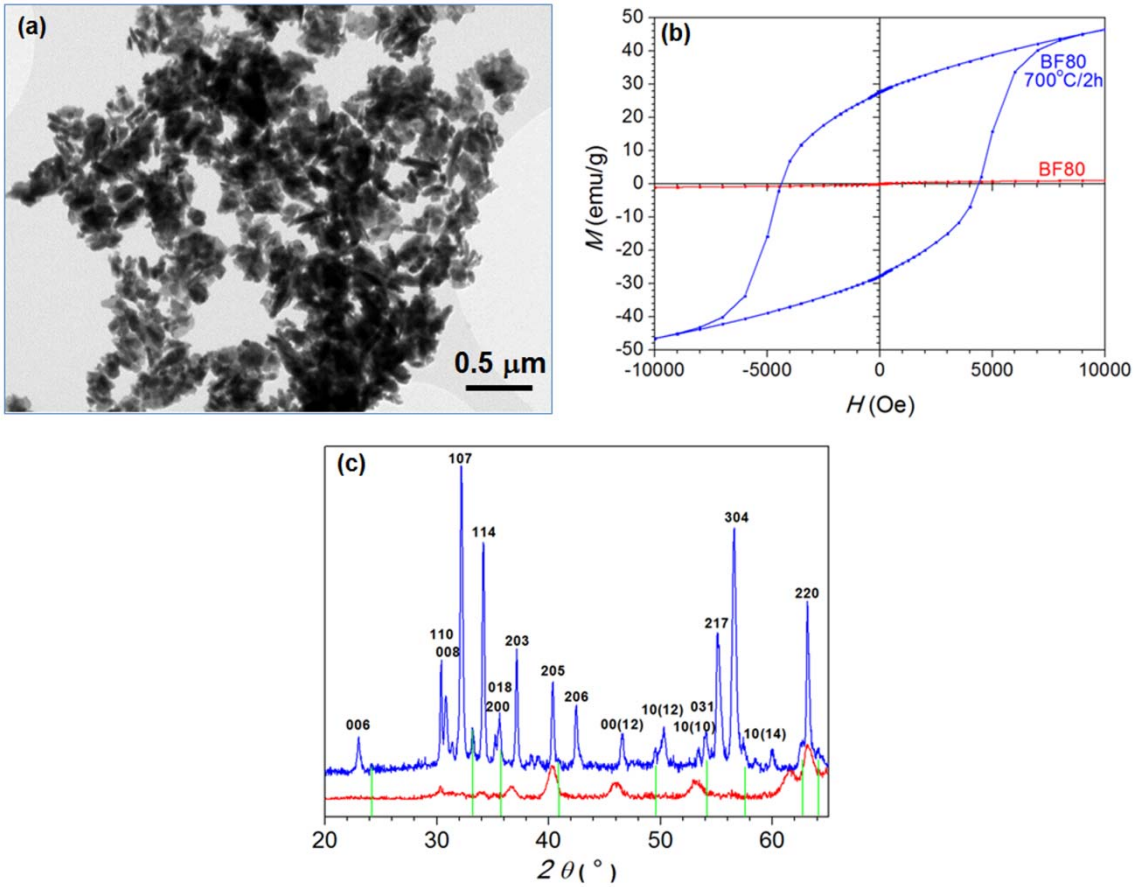

Fig. SI1 TEM image (a), room-temperature hysteresis (b) and XRD (c) for the nanoplatelets BF80 annealed for 2 hours at 700 ^{o}C. The red curves in (b) and (c) represent measurements for the original BF80 nanoplatelets before the annealing and the blue curves measurements for the annealed nanoplatelets. The diffractograms in (c) are indexed according to the M-hexaferrite structure and the green lines mark the positions of the hematite reflections.

The nanoplatelets were also annealed after they were coated with a thin, homogeneous silica layer.[S2] In short, to 80 mL of a suspension containing 400 mg of the BF80 nanoplatelets, 3.2 mL of aqueous suspension containing of 1.6 g of citric acid (CA) was added. The pH value was adjusted to pH 5.1 with 25% ammonium hydroxide. The suspension was then heated to 80 °C and vigorously stirred for 90 min and then cooled to room temperature, at that point the pH was increased to 10.1. The suspension was then sedimented with a centrifuge to remove the excess CA and re-dispersed in a dilute ammonia solution at pH 10.1. To the 100 Ml of formed stable suspension containing 40 mg CA-adsorbed nanoplatelets 25 mL of ethanol solution containing 7.46 mmol of tetraethyl orthosilicate (TEOS) was added. The coating reaction was catalysed by the addition of 1% of concentrated ammonium hydroxide. After the reaction mixture was stirred overnight, the silica-coated nanoplatelets (BF80-SIL) were sedimented, thoroughly washed with water and dried in the vacuum at room temperature. The powder was annealed for 2 hours at 700 ^{o}C in ambient air.

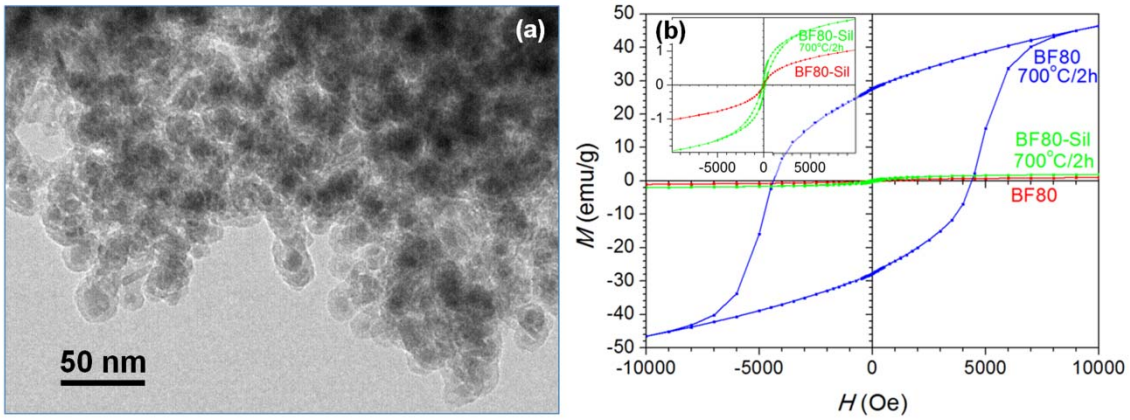

Fig. SI2 (a) TEM image of silica-coated nanoplatelets BF80 annealed for 2 hours at 700 ^{o}C, and (b) magnetic hystereses for the silica-coated nanoplatelets BF80-Sil before and after the annealing are compared with the hysteresis for the annealed uncoated nanoplatelets BF80.

EELS analysis of the Fe valence state across the nanoplatelet

Many methods have been reported to relate the energyloss near-edge structure (ELNES) of the L2,3 edges (2p $\rightarrow$ 3d - like transitions) to the valence state of the transition cations.[S3] For a determination of the Fe valence, two complementary methods are normally used, i.e., the Fe L_3/L_2 intensity ratio and the energy difference between O K and Fe L_3 edges ΔE.[S2,S4-S6] The chemical shift of the Fe L_3, L_2 edges is mainly influenced by the Fe valence state, whereas the L_3/L_2 intensity ratios additionally depend significantly on the coordination of the cations (in hexaferrites the Fe cations occupy three different lattice sites: octahedral, tetrahedral and trigonal). The EELS spectra were taken in the middle of the R block, in the middle of the S block and at the very surface of the nanoplatelets (see Figs. SI3 and SI4). The ΔE values measured in the spectra taken at different locations across the nanoplatelets varied slightly; however, the variations were with the expected experimental uncertainty of the measurement. The ΔE values for the nanoplatelets were similar to the ΔE measured from the spectrum of the hematite (α-Fe_2O_3) standard, suggesting an average valence state close to 3+ (see Table SI1 and Figs. SI3 and SI4).

Table SI1. Energy difference between O K and Fe L_3 edge (ΔE) from the EELS spectra taken at different areas of the nanoplatelet (see Fig. SI1).

Standard	Velence	ΔE (eV)
Fe_2O_3 (hematite)	3+	175.75±0.50
$FeTiO_3$ (ilmenite)	2+	174.00±0.50

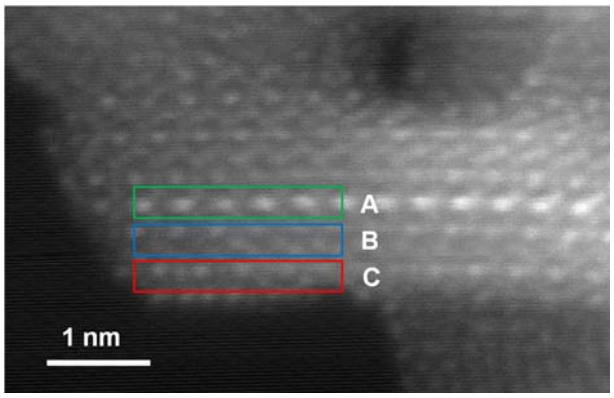

Position	ΔE (eV)
A - middle of R block	175.50±0.50
B - middle of S block	175.25±0.50
C - surface	175.00±0.50

Fig. SI3 HAADF STEM image of hexaferrite nanoplatelet BF80. Table on right lists energy difference between O K and Fe L_3 edge onsets (ΔE) measured from the EELS spectra taken at different areas of the nanoplatelet marked with rectangles on the HAADF image.

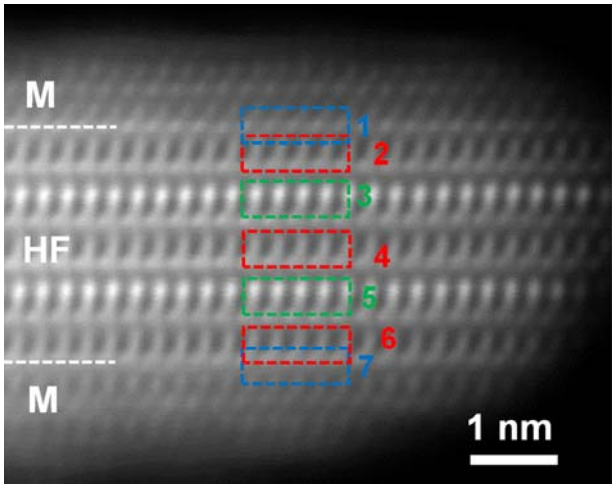

Position	ΔE (eV)
1 - interface	175.50±0.50
2 - middle of S block	175.75±0.50
3 - middle of R block	176.00±0.50
4 - middle of S block	176.00±0.50
5 - middle of R block	176.50±0.50
6 - middle of S block	175.75±0.50
7 - interface	176.25±0.50

Fig. SI4 HAADF STEM image of hexaferrite nanoplatelet from a BF160 sample. Table on right lists energy difference between O K and Fe L_3 edge onsets (ΔE) measured from the EELS spectra taken at different areas of the nanoplatelet marked with rectangles on the HAADF image.

Imaging of the nanoplatelet structure after the deposition of epitaxial maghemite layers onto their basal surfaces

The epitaxial layers of maghemite were deposited onto the basal surfaces of the hexaferrite nanoplatelets using the controlled co-precipitation of the Fe^{3+}/Fe^{2+} ions in their aqueous suspension.[S7] The complete procedure is given in reference 36. In brief, the nanoplatelets BF160 (40 mg) were dispersed in dilute nitric acid (80 mL) at a pH of 4.5. The suspension was heated to 60 °C in an argon flow. Then, $[Fe((H_2N)_2C=O)_6](NO_3)_3$ (0.18 mmol) and $FeCl_2$ (0.9 mmol) were dissolved in the suspension and stirred. After 10 minutes solid $Mg(OH)_2$ (0.48 mmol) was added to the suspension to increase the pH. After aging for 2 h at 60 °C the reaction mixture was allowed to cool naturally to room temperature.

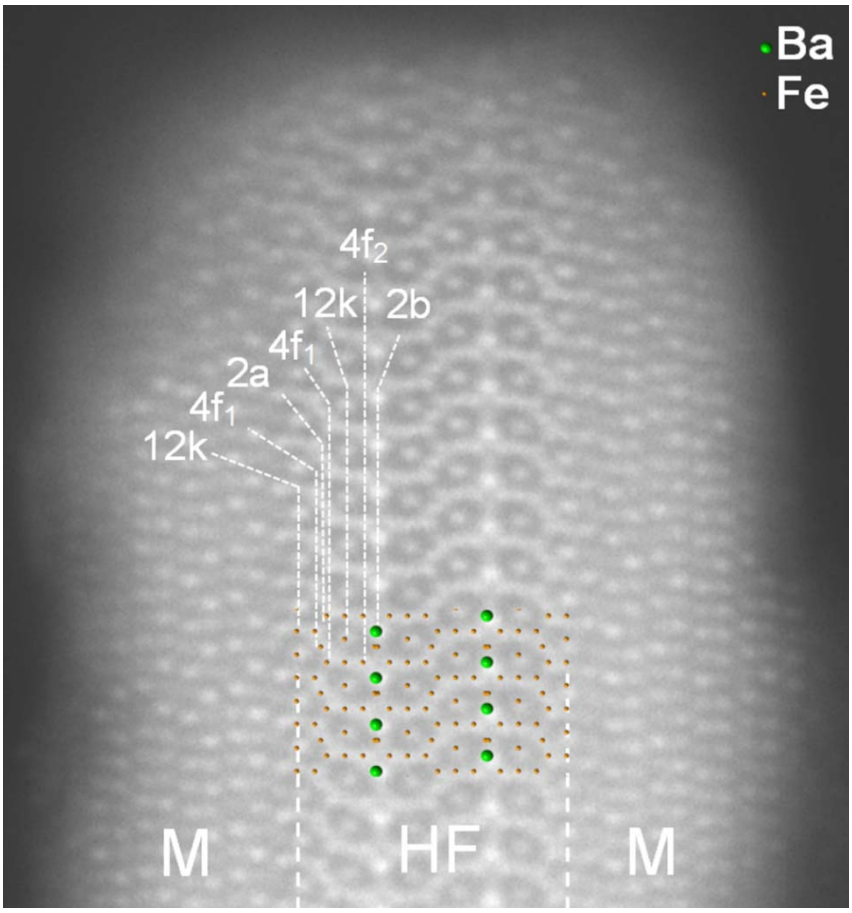

Fig. SI5 HAADF STEM image of hexaferrite (HF) nanoplatelet with epitaxial maghemite (M) layers growing at its basal surfaces The hexaferrite structure projected along <10-10> is superimposed over the image to illustrate the positions of the Ba^{2+} and Fe^{3+} ions. Different Fe lattice sites in the hexaferrite structure (i.e., trigonal 2b, tetrahedral $4f_1$, octahedral 12k, 2a, and $4f_2$) are marked.

EDXS elemental mapping of as-synthesized BF80 nanoplatelets

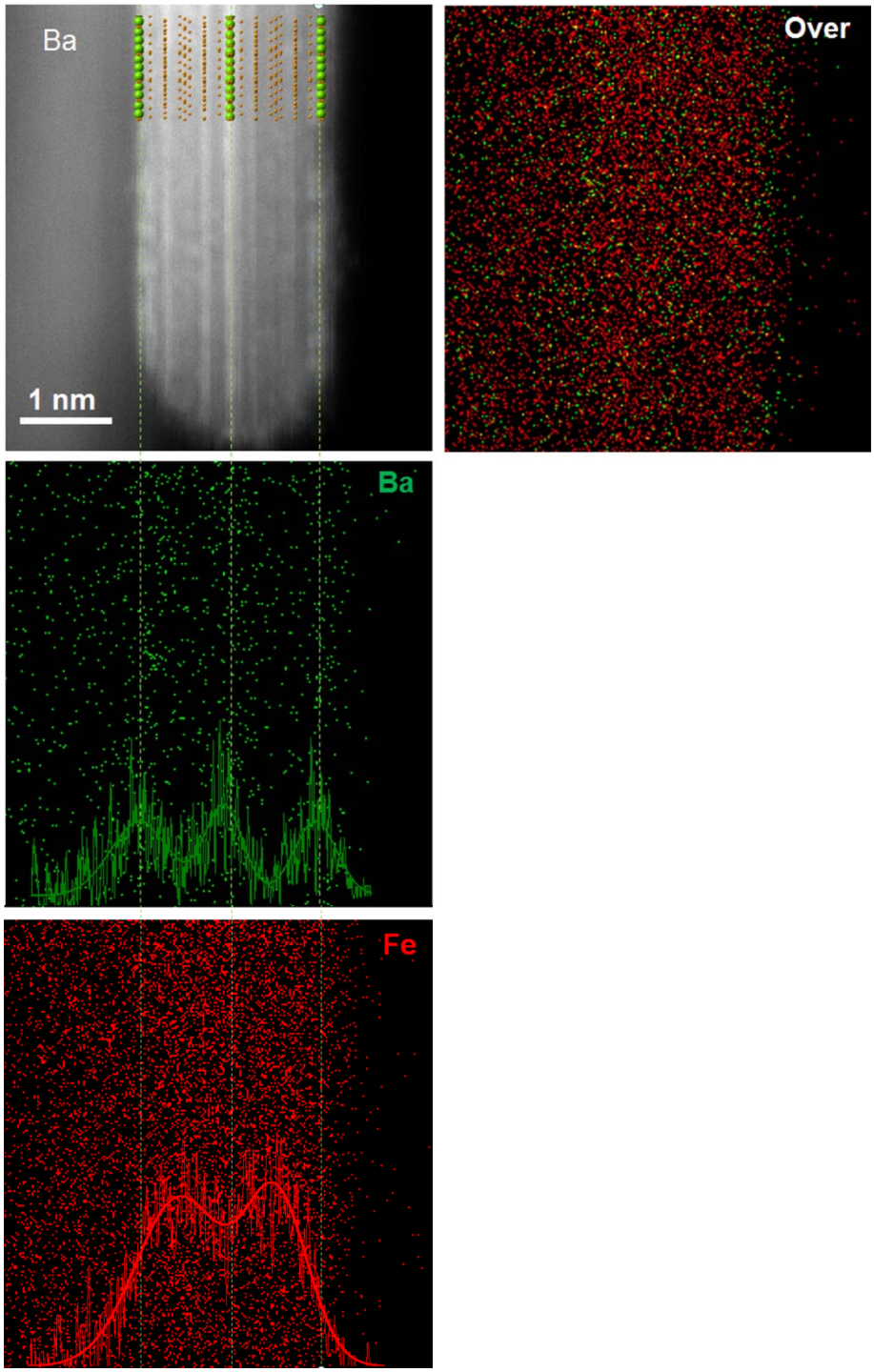

Fig. SI6 HAADF STEM image with the corresponding EDX elemental maps for Ba and Fe of a nanoplatelet oriented with basal planes parallel to the electron beam. The nanoplatelet was extracted from the BF80 sample before the product was washed with diluted nitric acid. The intensity profiles showing the distribution of the two elements across the nanoplatelet are superimposed over the elemental maps.

Ab-initio calculations

The stabilities of the structures with respect to various termination planes were theoretically investigated by means of *ab-initio* calculations of the total energies within the framework of the density-functional theory.[S8-S10] The considered models were constructed by terminating the structure at different atomic planes symmetrically to the central Ba/O/Fe(2b) plane (Fig. 4(c)). The stacking sequence is continued by the vacuum layers of the thicknesses matching the distance between the two termination planes. The initial super-cells were constructed by adopting the experimental lattice parameters for the bulk barium hexaferrite.

The calculations were carried out by applying the Quantum Espresso[S8] code. The interaction between the core and valence electrons was described by the Troullier-Martins-type[S9] pseudopotential, whereas the exchange-correlation effects were treated within the generalized-gradient approximation (GGA)[S10]. The wave functions and the charge densities were expanded in the plane waves with the cut-off parameters 272 eV and 1088 eV, respectively, and the 4×4×1 mesh was used for the Brillouin zone integration. The structures were optimized by modifying the initial atomic positions to correspond to the states with no strain and minimal total energies.

The calculated total energies for the different model structures are not directly comparable due to the varying number of atoms. For that reason, we define the total-energy density **e**, as the resulting energy **E**, divided by the number $\mathbf{N_{Ba}}$, $\mathbf{N_{Fe}}$, $\mathbf{N_O}$ of the particular-type atoms, $\mathbf{e}=\mathbf{E}/(\mathbf{N_{Ba}}+\mathbf{N_{Fe}}+\mathbf{N_O})$. The lowest $\mathbf{e_0}$ corresponds to the system with the O-plane "e" of the S block (see Fig. 4(c)).

References

S1. H. Tan, J. Verbeeck, A. Abakumov and G. van Tendeloo, *Ultramicrosocpy*, 2012, **116**, 24-33.

S2. S. Kralj, D. Makovec, S. Čampelj and M. Drofenik, *J. Magn. Magn. Mater.*, 2010, **322**, 1847–1853.

S3. L. Yedra, E. Xuriguera, M. Estrader, A. López-Ortega, M. D. Baró, J. Nogués, M. Roldan, M. Varela, S. Estradé and F. Peiró, *Micros. Microanal*., 2014, **20**, 698-706.

S4. J.Taftø and O. L. Krivanek, *Phys. Rev. Lett*., 1982, **48**, 560-563.

S5. H. K. Schmidt and W. Mader, *Micron.*, 2006, **37**, 426-432.

S6. S. Gyergyek, D. Makovec, M. Jagodič, M. Drofenik, K. Schenk, O. Jordan, J. Kovač, G. Dražić and H. Hofmann, *J. Alloys Compd*., 2017, **694**, 261-271.

S7. B. Belec, G. Dražić, S. Gyergyek, B. Podmiljšak, T. Goršak, M. Komelj, J. Nogués and D. Makovec, *Nanoscale*, 2017, **9**, 17551–17560.

S8. P. Giannozzi, S. Baroni, N. Bonini, M. Calandra, R. Car, C. Cavazzoni, D. Ceresoli, G. L. Chiarottia, M. Cococcioni, I. Dabo, A. D. Corso, S. Fabris, G. Fratesi, S. de Gironcoli, R. Gebauer, U. Gerstmann, C. Gougoussis, A. Kokalj, M. Lazzeri, L. Martin-Samos, N. Marzari, F. Mauri, R. Mazzarello, S. Paolini, A. Pasquarello, L. Paulatto, C. Sbraccia, S. Scandolo, G. Sclauzero, A. P. Seitsonena, A. Smogunov, P. Umari and R. M. Wentzcovitch, *J. Phys. Condens. Matter*, 2009, **21**, 395502-1-395502-19.

S9. J. Troullier and J.L. Martins, *Phys. Rev.*, 1991, **B43**, 1993-2006.

S10. J. P. Perdew, K. Burke and M. Ernzerhof, *Phys. Rev. Lett.*, 1996, **77**, 3865-3868.